

# Longitudinal Nonreciprocal Charge Transport with Time Reversal Symmetry

Harsh Varshney\* and Amit Agarwal†

Department of Physics, Indian Institute of Technology, Kanpur-208016, India.

Longitudinal nonreciprocal charge transport is widely believed to require time-reversal symmetry breaking, either in magnetic materials or through external magnetic fields. Here, we show that longitudinal nonreciprocity can arise even in nonmagnetic conductors without magnetic fields through disorder-induced asymmetric scattering. Using a semiclassical Boltzmann framework, we develop a general theory in which skew-scattering and side-jump processes generate a nonlinear longitudinal current that remains finite even in time-reversal-symmetric systems. A systematic symmetry analysis identifies 42 point groups that permit this extrinsic mechanism. As a concrete realization, we demonstrate that Bernal-stacked bilayer graphene exhibits a large and gate-tunable longitudinal nonreciprocal response with a sizable nonreciprocity factor near its Lifshitz transition. These results establish disorder-driven asymmetric scattering as a general mechanism for bulk longitudinal nonreciprocal charge transport in crystalline conductors.

**Introduction:**— Nonreciprocal charge transport (NCT), the asymmetric electrical response under current or field reversal, is a fundamental nonlinear transport phenomenon that arises in noncentrosymmetric systems [1–8]. In two-terminal geometries, NCT manifests as a longitudinal effect in which oppositely directed currents experience different resistances. While strong nonreciprocity is routinely achieved in junction-based devices, realizing such behavior intrinsically in bulk crystalline materials remains fundamentally challenging. In crystalline conductors, longitudinal nonreciprocity is widely believed to require the simultaneous breaking of inversion and time-reversal ( $\mathcal{T}$ ) symmetries, typically realized in magnetic materials or under external magnetic fields [4, 9, 10]. This constraint severely limits the realization of longitudinal NCT in nonmagnetic systems and motivates the search for alternative microscopic mechanisms that can generate nonreciprocity in time-reversal-symmetric conductors.

Recent studies have shown that materials lacking both inversion and time-reversal symmetries can exhibit longitudinal NCT through second-order nonlinear conductivity [3, 6, 9–21]. Proposed mechanisms include electrical magnetochiral anisotropy [1, 2, 22–24], nonlinear Drude contributions [24–26], intrinsic band-geometry effects governed by Berry-connection polarizability [24, 27–30], and Lorentz-force-induced skew scattering [31, 32]. However, all of these mechanisms require broken time-reversal symmetry ( $\mathcal{T}$ ) and therefore vanish in systems that preserve it (see Fig. 1). It is therefore widely believed that longitudinal NCT requires simultaneous breaking of inversion and time-reversal symmetries [4, 9, 10]. This constraint excludes a broad class of nonmagnetic materials and raises a fundamental question: can longitudinal nonreciprocity arise without breaking time-reversal symmetry?

In this Letter, we show that longitudinal NCT can arise even in  $\mathcal{T}$ -symmetric noncentrosymmetric conductors (Fig. 1). The key ingredient is impurity-induced asymmetric scattering, which generates nonlinear skew-

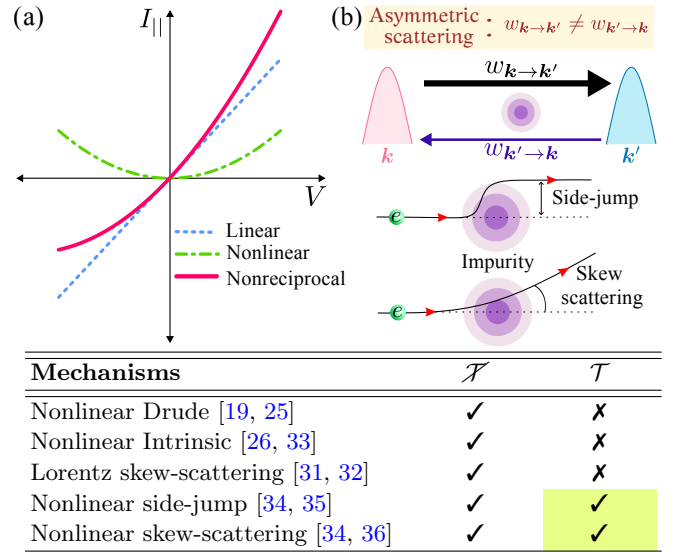


FIG. 1. **Longitudinal nonreciprocal transport without magnetic fields.** (a) Schematic  $I_{\parallel}$ - $V$  characteristics illustrating linear, nonlinear, and resulting nonreciprocal responses. A second-order contribution makes the forward and reverse currents unequal, producing a nonreciprocal current response. (b) Microscopic mechanism. In noncentrosymmetric systems, asymmetric impurity scattering mechanisms such as skew-scattering and side-jump generate a longitudinal current  $\propto E^2$ , even when time-reversal symmetry ( $\mathcal{T}$ ) is preserved. The table summarizes known mechanisms for longitudinal nonlinear transport and shows that extrinsic scattering processes enable nonreciprocity in nonmagnetic materials.

scattering and nonlinear side-jump contributions [20, 34, 36–41]. These processes produce a longitudinal current quadratic in the electric field ( $\propto E^2$ ) while preserving time-reversal symmetry [35, 42–44]. These NCT responses are consistent with Onsager reciprocity, detailed balance, and microscopic reversibility (see Appendix A1 and A2).

Our symmetry analysis across all 122 point groups identifies 42 crystal classes that permit such time-

reversal-symmetric longitudinal NCT. As a concrete realization, we demonstrate this mechanism in gated Bernal-stacked bilayer graphene (BLG), which preserves time-reversal symmetry. A perpendicular electric field breaks inversion symmetry and enables a large, gate-tunable nonreciprocal response. The predicted magnitude and tunability are consistent with recent experimental observations [43–45]. These results establish disorder-driven asymmetric scattering as a general mechanism for bulk longitudinal nonreciprocal charge transport in crystalline conductors.

*Origin of longitudinal nonlinear nonreciprocity:*—The charge current in a quasiparticle system is given by,  $\mathbf{j} = -e \sum_{\mathbf{k}} \mathbf{v}_{\mathbf{k}} f_{\mathbf{k}}$ , where  $\mathbf{v}_{\mathbf{k}}$  is the band velocity and  $f_{\mathbf{k}}$  is the distribution function. Under an applied electric field, both quantities acquire field-induced corrections. Expanding both quantities in powers of the electric field, we can express the second-order current as

$$\mathbf{j}^{(2)} = -e \sum_{\mathbf{k}} \left[ \mathbf{v}_{\mathbf{k}}^{(0)} f_{\mathbf{k}}^{(2)} + \mathbf{v}_{\mathbf{k}}^{(1)} f_{\mathbf{k}}^{(1)} + \mathbf{v}_{\mathbf{k}}^{(2)} f_{\mathbf{k}}^{(0)} \right]. \quad (1)$$

For a finite response proportional to  $E^2$ , the integrand must be even under momentum inversion  $\mathbf{k} \rightarrow -\mathbf{k}$ . In time-reversal-symmetric systems, the equilibrium distribution  $f_{\mathbf{k}}^{(0)}$  is even in momentum while the band velocity  $\mathbf{v}_{\mathbf{k}}^{(0)}$  is odd. Intrinsic electric-field corrections to the velocity,  $\mathbf{v}_{\mathbf{k}}^{(1)}$  and  $\mathbf{v}_{\mathbf{k}}^{(2)}$ , are also odd in  $\mathbf{k}$  [27, 46]. Consequently the intrinsic contribution to  $\mathbf{v}_{\mathbf{k}}^{(2)} f_{\mathbf{k}}^{(0)}$  remains odd and vanishes after Brillouin-zone integration.

The first-order nonequilibrium distribution [47] satisfies  $f_{\mathbf{k}}^{(1)} \propto \mathbf{E} \cdot \mathbf{v}_{\mathbf{k}}^{(0)}$ , and it is therefore odd in momentum. Although the product  $\mathbf{v}_{\mathbf{k}}^{(1)} f_{\mathbf{k}}^{(1)}$  is even, the intrinsic velocity correction  $\mathbf{v}_{\mathbf{k}}^{(1)} \propto \mathbf{E} \times \boldsymbol{\Omega}_{\mathbf{k}}$  is transverse to the applied field and produces nonlinear Hall responses rather than a longitudinal NCT. The remaining term  $\mathbf{v}_{\mathbf{k}}^{(0)} f_{\mathbf{k}}^{(2)}$  can generate a longitudinal nonlinear current. Since  $\mathbf{v}_{\mathbf{k}}^{(0)}$  is odd in momentum, this requires a  $\mathbf{k}$ -odd component in  $f_{\mathbf{k}}^{(2)}$ . However, such a contribution is absent within the conventional symmetric scattering approximations, such as relaxation-time, where  $w_{\mathbf{k} \rightarrow \mathbf{k}'} = w_{\mathbf{k}' \rightarrow \mathbf{k}}$ . For such symmetric scattering,  $f_{\mathbf{k}}^{(2)}$  remains even in momentum unless time reversal symmetry is broken, leading to a vanishing longitudinal nonlinear current. This has led to the common belief that longitudinal nonreciprocity is forbidden in time-reversal-symmetric conductors.

We show that this restriction is lifted once disorder-induced asymmetric scattering is included. In noncentrosymmetric systems, the scattering probability contains an antisymmetric component satisfying  $w_{\mathbf{k} \rightarrow \mathbf{k}'} \neq w_{\mathbf{k}' \rightarrow \mathbf{k}}$ , while maintaining microscopic reversibility and detailed balance (see Appendix A2). Such asymmetric scattering generates a  $\mathbf{k}$ -odd component of  $f_{\mathbf{k}}^{(2)}$ , which combines with the  $\mathbf{k}$ -odd band velocity to produce a fi-

nite longitudinal current proportional to  $E^2$ . Two extrinsic mechanisms naturally generate this asymmetry. Skew scattering produces a directional imbalance in impurity scattering that directly induces a  $\mathbf{k}$ -odd correction to the distribution function. In addition, impurity scattering can produce a real-space coordinate shift of the electronic wave packet, giving rise to a side-jump velocity and additional corrections to the distribution. Both mechanisms provide robust microscopic channels for longitudinal nonreciprocal charge transport even in time-reversal-symmetric systems.

*Disorder-driven longitudinal nonreciprocity:*—In a two-terminal geometry, we can express the longitudinal electric current up to second-order as,

$$j_a = \sigma_{aa}^{\text{eff}} E_a \quad \text{where} \quad \sigma_{aa}^{\text{eff}}(\mathbf{E}) \equiv \sigma_{aa} + \sigma_{aaa} E_a. \quad (2)$$

Here,  $\sigma_{aa}$  and  $\sigma_{aaa}$  denote the linear and second-order conductivity tensors, whereas  $\sigma_{aa}^{\text{eff}}(\mathbf{E})$  represent the total effective conductivity. The nonlinear conductivity  $\sigma_{aaa}$  controls the magnitude of longitudinal nonreciprocal charge transport. To calculate these conductivities, we use the semiclassical expression for the current,  $\mathbf{j} = -e \sum_l \dot{\mathbf{r}}_l f_l$ , where  $l = (n, \mathbf{k})$  labels a Bloch state and  $\dot{\mathbf{r}}_l$  is the wave-packet velocity. The nonequilibrium distribution function  $f_l$  is obtained from the steady-state Boltzmann equation in a homogeneous field,  $\dot{\mathbf{k}} \cdot \nabla_{\mathbf{k}} f_l = I_{\text{el}}[f_l]$ , with  $\hbar \dot{\mathbf{k}} = -e \mathbf{E}$  and  $I_{\text{el}}$  the elastic collision integral [47].

In real materials, impurity scattering transfers electrons between states  $l$  and  $l'$  with scattering rate probability  $w_{ll'} \equiv w_{l \rightarrow l'}$ . In noncentrosymmetric systems, this scattering rate can generally be decomposed into symmetric ( $w_{ll'}^S$ ) and antisymmetric parts ( $w_{ll'}^A$ ),

$$w_{ll'} = w_{ll'}^S + w_{ll'}^A, \quad \text{where,} \quad w_{ll'}^{S/A} = \frac{w_{ll'} \pm w_{l'l}}{2}, \quad (3)$$

The symmetric part describes conventional momentum relaxation, whereas the antisymmetric part arises from extrinsic skew scattering and side-jump processes. In addition, extrinsic impurity scattering also induces a real-space shift of the electronic wave packet during a collision, generating a side-jump velocity.

Including these disorder-induced processes, the electrical conductivity can be expressed as,

$$\sigma_{aaa} = \sigma_{aaa}^{\text{ND}} + \sigma_{aaa}^{\text{NSJ}} + \sigma_{aaa}^{\text{NSK}}, \quad (4)$$

where  $\sigma^{\text{ND}}$ ,  $\sigma^{\text{NSJ}}$ , and  $\sigma^{\text{NSK}}$  denote the nonlinear Drude, side-jump, and skew-scattering contributions, respectively. In  $\mathcal{T}$ -symmetric systems, the linear conductivity solely arises from the Drude contribution ( $\sigma_{aa}^{\text{D}}$ ), whereas nonlinear longitudinal conductivity originates from side-jump and skew-scattering contributions, which dominate the longitudinal NCT.

Solving the Boltzmann equation beyond the relaxation-time approximation (see Sec. 1 of the

TABLE I. List of all 42 point groups (both nonmagnetic and magnetic) that allow a finite  $\mathcal{T}$ -even longitudinal conductivity  $\sigma_{aaa}$ . While our focus is on nonmagnetic systems, the contributions of  $\sigma^{\text{NSJ}}$  and  $\sigma^{\text{NSK}}$  in magnetic systems also remain largely unexplored.

$\mathcal{T}$ -even $\sigma_{aaa}$	Nonmagnetic point groups	Magnetic point groups
$\sigma_{xxx}$	1, $m$ , 3, 32, $-6$	1.1', $m.1'$ , $m'$ , 3.1', 32.1', 32', $-6.1'$ , $-6'$
$\sigma_{yyy}$	1, 2, 3, $3m$ , $-6$ , $-6m2$	1.1', 2.1', 2', 3.1', 3 $m.1'$ , 3 $m'$ , $-6.1'$ , $-6'$ , $-6m2.1'$ , $-6m'2'$ , $-6'm2'$ , $-6'm'2$
$\sigma_{zzz}$	1, $m$ , $mm2$ , 4, $4mm$ , 3, 3 $m$ , 6, $6mm$	1.1', $m.1'$ , $m'$ , $mm2.1'$ , $m'm'2$ , $m'm'2'$ , 4.1', 4', 4 $mm.1'$ , 4 $m'm'$ , 4' $m'm'$ , 3.1', 3 $m.1'$ , 3 $m'$ , 6.1', 6', 6 $mm.1'$ , 6 $m'm'$ , 6' $mm'$

Supplemental Material (SM) [48] for details), we obtain linear Drude and nonlinear side-jump and skew scattering conductivities as

$$\sigma_{aa}^{\text{D}} = -e^2 \tau \sum_l v_l^a v_l^a \partial_{\epsilon_l} f_l^0, \quad (5a)$$

$$\sigma_{aaa}^{\text{NSJ}} = -\frac{2e^3 \tau^2}{\hbar} \sum_l v_l^{\text{sj},a} \partial_a v_l^a \partial_{\epsilon_l} f_l^0, \quad (5b)$$

$$\sigma_{aaa}^{\text{NSK}} = \frac{e^3 \tau^3}{\hbar^2} \sum_{l,l'} w_{ll'}^A [v_l^a \partial_a^2 f_l^0 - (\partial_a' v_{l'}^a) \partial_a f_l^0]. \quad (5c)$$

Here,  $v_l^a = \hbar^{-1} \partial_{k_a} \epsilon_l$  is the group velocity and  $f_l^0$  is the equilibrium Fermi-Dirac distribution. The side-jump velocity is defined as  $\mathbf{v}_l^{\text{sj}} = -\sum_{l'} w_{ll'}^S \delta \mathbf{r}_{ll'}$ , where  $\delta \mathbf{r}_{ll'}$  is the coordinate shift of the wave packet during scattering [49]. Importantly, both  $\sigma^{\text{NSJ}}$  and  $\sigma^{\text{NSK}}$  are  $\mathcal{T}$ -even responses, consistent with microscopic reversibility, allowing them to remain finite in  $\mathcal{T}$ -symmetric systems.

Although these contributions originate from disorder, their magnitude is closely linked to the underlying band geometry. In particular, both the side-jump velocity and the antisymmetric scattering rate are controlled by the Berry curvature of the electronic bands [50]. We show and discuss the band geometric origin of the coordinate shift and skew-scattering rate explicitly in Appendix A3. Thus, longitudinal nonlinear conductivity offers an independent probe of band geometry, even in systems where the nonlinear Hall response may vanish due to crystalline symmetries. Materials with strong Berry curvature and inversion symmetry breaking provide natural platforms for large disorder-driven longitudinal NCT.

**Symmetry constraints on nonreciprocity:**— The longitudinal nonlinear conductivity  $\sigma_{aaa}$  is strongly constrained by crystal symmetry. In particular, inversion symmetry forces  $\sigma_{aaa}$  to vanish. Consequently, noncen-

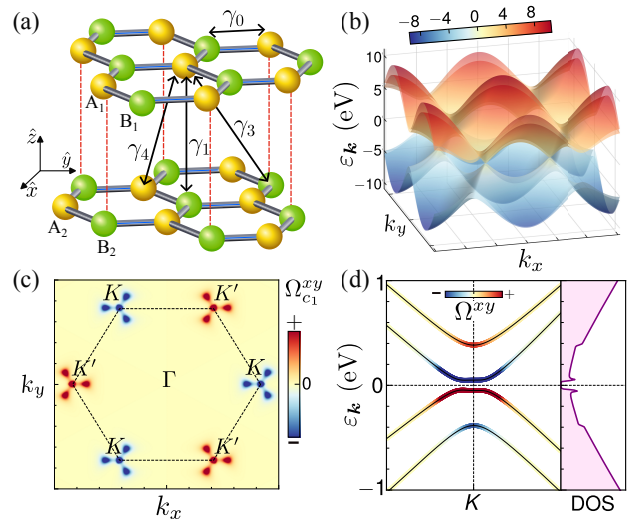


FIG. 2. **Bernal-stacked bilayer graphene (BLG) and its electronic properties.** (a) Crystal structure of BLG showing the AB stacking and the relevant intra- and interlayer hopping processes. (b) Electronic band dispersion of BLG. (c) Berry curvature distribution of the first conduction band in momentum space, exhibiting pronounced hot spots near the  $K$  and  $K'$  valleys. The dashed hexagon indicates the first Brillouin zone with marked high-symmetry points. (d) Band structure near the  $K$  valley, color-coded by the Berry curvature magnitude, together with the density of states. BLG parameters are discussed in Sec. S2 of the SM [48], and the onsite potential is  $\Delta = 0.05$  eV.

trosymmetric materials are a necessary condition for observing longitudinal nonreciprocity.

As discussed in Eq. (4), the total nonlinear conductivity contains contributions that behave differently under time reversal. The nonlinear Drude term  $\sigma_{aaa}^{\text{ND}}$  is odd under time reversal, and it requires broken  $\mathcal{T}$  to be finite. In contrast, the disorder-induced side-jump and skew-scattering contributions  $\sigma_{aaa}^{\text{NSJ}}$  and  $\sigma_{aaa}^{\text{NSK}}$  are  $\mathcal{T}$ -even and can remain finite in nonmagnetic systems. Consequently, inversion symmetry breaking alone is sufficient to allow longitudinal NCT driven by these extrinsic mechanisms.

To identify candidate materials that support the  $\mathcal{T}$ -even  $\sigma_{aaa}^{\text{NSJ}}$  and  $\sigma_{aaa}^{\text{NSK}}$  contributions, we perform a systematic symmetry analysis across all 122 point groups. Following Neumann's principle [51] and using the Bilbao Crystallographic Server [52], we identify 42 point groups (including magnetic materials) that permit a nonvanishing  $\sigma_{aaa}$ . The resulting classification is summarized in Table I. The table highlights several experimentally relevant noncentrosymmetric point groups, such as 3.1', 3 $m.1'$ ,  $-6.1'$ , and  $-6'$ , which permit  $\mathcal{T}$ -even nonlinear conductivity and support sizable longitudinal NCT signals while preserving time reversal symmetry. Prominent material platforms include Weyl semimetals [53, 54], tellurium [55, 56], graphene layers and their heterostructures [35, 43, 44, 57–59], and Rashba systems [60].

*Large longitudinal nonreciprocity in BLG:*— To illustrate the magnitude of longitudinal NCT response, we consider Bernal-stacked bilayer graphene (BLG), shown in Fig. 2(a). BLG provides an ideal platform because its carrier density and inversion asymmetry can be independently tuned in a dual-gate device. A vertical displacement field breaks inversion symmetry while preserving time-reversal symmetry. The crystalline symmetry of gated BLG further constrains the allowed nonlinear conductivities. Even in the presence of a displacement field, BLG preserves  $\mathcal{T}$  and  $\mathcal{C}_{3z}$  symmetries, and belongs to the  $3m.1'$  point group. Consequently, the  $\mathcal{T}$ -odd nonlinear Drude contribution vanishes, whereas the  $\mathcal{T}$ -even side-jump and skew-scattering mechanisms contribute to longitudinal NCT. In addition, BLG retains a mirror symmetry  $\mathcal{M}_x$  about the armchair direction (see Fig. S1 of the SM [48]), which forces  $\sigma_{xxx} = 0$ . Therefore, the only symmetry-allowed longitudinal NCT response in pristine BLG is  $\sigma_{yyy}$ , consistent with Table I.

We follow Refs. [61–63] for the tight-binding model of AB-stacked BLG that captures the electronic structure, including the low-energy bands near the Dirac points (details in Sec. S2 of the SM [48]). The resulting dispersion is shown in Fig. 2(b). The displacement-field breaks inversion symmetry and generates a finite Berry curvature, concentrated near the  $K$  and  $K'$  valleys [Fig. 2(c)]. The band structure around the  $K$  valley, weighted by Berry curvature, together with the density of states, is shown in Fig. 2(d). Trigonal warping produces low-energy van Hove singularities near the band edges, giving rise to pronounced peaks in the density of states (see Sec. S3 of the SM [48] for details).

We next evaluate the dependence of linear and nonlinear conductivities on the experimentally controllable chemical potential  $\mu$  and displacement-field potential  $\Delta$ . The results are presented in Fig. 3. Van Hove singularities near the band edges strongly enhance the nonlinear conductivities, while the linear conductivity remains smooth and nearly symmetric in  $\mu$  and  $\Delta$ . The side-jump contribution  $\sigma_{yyy}^{\text{NSJ}}$  [Fig. 3(c)] is symmetric in  $\mu$  and antisymmetric in  $\Delta$ . In contrast, the skew-scattering contribution  $\sigma_{yyy}^{\text{NSK}}$  [Fig. 3(d)] is antisymmetric in both  $\mu$  and  $\Delta$  and changes sign across the van Hove singularities. For the typical disorder parameters used here, the skew-scattering term dominates the nonlinear response. Details of the disorder modeling and parameters are presented in Appendix A3. The strong enhancement of longitudinal NCT near van Hove singularities, together with gate tunability, makes BLG particularly suitable for experimental observation of longitudinal NCT.

*Experimental signature of NCT in BLG:*— To quantify the magnitude of longitudinal nonreciprocity, we introduce the dimensionless nonreciprocity factor [31],

$$\eta = \left| \frac{\sigma^{\text{eff}}(E_a) - \sigma^{\text{eff}}(-E_a)}{\sigma^{\text{eff}}(E_a) + \sigma^{\text{eff}}(-E_a)} \right| = \left| \frac{\sigma_{aaa} E_a}{\sigma_{aa}} \right| \equiv \left| \frac{V_{aa}^{2\omega}}{V_{aa}^\omega} \right|. \quad (6)$$

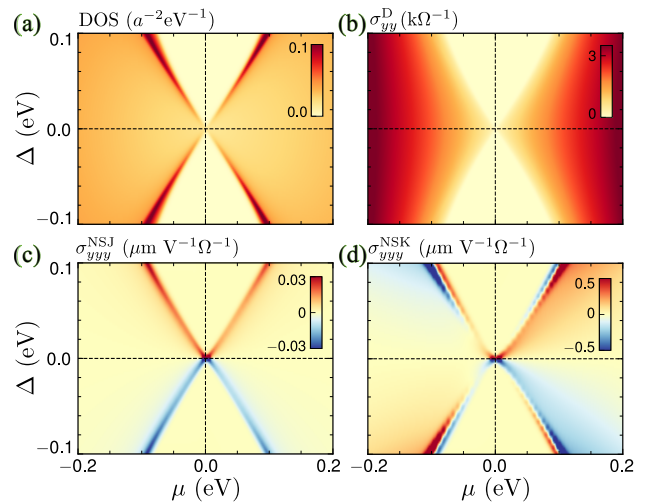


FIG. 3. **Linear and nonlinear conductivities in bilayer graphene in the  $\mu$ - $\Delta$  plane.** (a) Density of states, showing van Hove singularities near the band edges. (b) Linear Drude conductivity  $\sigma_{yy} = \sigma_{xx}$ . (c) Nonlinear side-jump contribution  $\sigma_{yyy}^{\text{NSJ}}$ . (d) Nonlinear skew-scattering contribution  $\sigma_{yyy}^{\text{NSK}}$ . We considered  $T = 20$  K with model parameters identical to Fig. 2.

Here,  $E_a$  is the magnitude of the applied electric field and  $\eta$  quantifies the asymmetry between forward and reverse currents. In nonlinear transport experiments, the response is detected through the first- and second-harmonic voltages  $V_{aa}^\omega$  and  $V_{aa}^{2\omega}$ . The conductivity ratio can be expressed in terms of these voltages as  $\sigma_{aaa} E_a / \sigma_{aa} = V_{aa}^{2\omega} / V_{aa}^\omega$  [43] (details in Sec. S4 of the SM [48]). This allows a direct estimation of the nonreciprocity factor from the measured harmonic voltages. For the asymmetric scattering mechanism, we analyze the disorder dependence of  $\eta$  in Sec. S5 of SM [48].

Using the calculated linear and nonlinear conductivities of bilayer graphene, we present the phase diagram of  $\eta$  in the  $(\mu, \Delta)$  plane in Fig. 4(a). A pronounced enhancement of  $\eta$  appears near the band edges, where van Hove singularities suppress the linear conductivity while enhancing the nonlinear response. As a result,  $\eta$  reaches values as large as  $\sim 0.4$ , corresponding to nearly 40% nonreciprocity for an experimentally accessible electric field  $E \sim 0.5$  V/nm. The nonreciprocity is also strongly tunable through the displacement field  $\Delta$ .

To test these predictions, we compare them with recent measurements of nonlinear longitudinal transport in bilayer graphene [44]. Figure 4(b) shows the measured  $V_{xx}^{2\omega}$  as a function of  $V_{xx}^\omega$  for several displacement fields  $D$ . Using Eq. (6), we convert these measurements into the corresponding nonreciprocity factor and present the results in Fig. 4(c). Consistent with our theoretical predictions,  $\eta$  increases monotonically with  $|\Delta|$  and reaches values of order  $\eta \sim 0.3$  ( $\sim 30\%$  nonreciprocity) for  $D/\epsilon_0 = -0.5$  V/nm [64]. This giant value of  $\eta$  in BLG

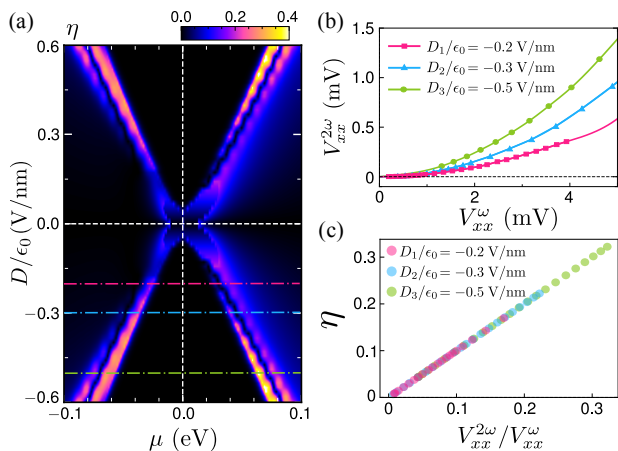


FIG. 4. **Large longitudinal nonreciprocity in gated bilayer graphene.** (a) Calculated nonreciprocity factor  $\eta$  as a function of chemical potential  $\mu$  and displacement field  $D$ . Strong nonreciprocity appears near the band edges, where linear conductivity is small and nonlinear conductivity is large. (b) Experimentally measured second-harmonic voltage  $V_{xx}^{2\omega}$  versus first-harmonic voltage  $V_{xx}^{\omega}$  for different displacement fields  $D$ , reproduced from Ref. [44]. (c) Nonreciprocity factor  $\eta$  extracted from the experimental data using Eq. (6), reaching values larger than  $\sim 30\%$ , consistent with theory.

originates from the combination of strong Berry curvature and van Hove singularities near the band edges.

Unlike nonlinear Hall responses, which probe Berry-curvature-dipole physics, the present mechanism arises directly in the longitudinal channel and is governed by asymmetric scattering. Despite extensive studies of nonlinear Hall transport in nonmagnetic systems, longitudinal NCT remains largely unexplored. Since nonreciprocity arises from the interplay of linear and nonlinear contributions, targeted longitudinal transport measurements probing the total response should directly reveal the predicted effect.

**Conclusion:**— We have shown that longitudinal nonreciprocal charge transport does not require time-reversal symmetry breaking. Instead, finite nonreciprocity can arise in noncentrosymmetric conductors through disorder-induced asymmetric scattering that preserves microscopic reversibility and detailed balance. In particular, nonlinear skew-scattering and side-jump processes generate a longitudinal current proportional to  $E^2$ .

A systematic symmetry analysis identifies 42 point groups that allow such time-reversal-symmetric longitudinal nonreciprocity. As a concrete realization, we demonstrate that gated Bernal-stacked bilayer graphene supports a very large and gate-tunable nonreciprocal response. The nonreciprocity factor in BLG approaches  $\sim 40\%$  due to the simultaneous enhancement of nonlinear transport and suppression of linear transport near van Hove singularities, consistent with recent experiments. More broadly, our results establish disorder-driven asym-

metric scattering as a general mechanism for bulk longitudinal nonreciprocal charge transport in crystalline solids.

**Acknowledgment:**— We acknowledge Tanweer Ahmed, Luis E. Hueso, Kamal Das, Sunit Das, and Sayan Sarkar for many fruitful discussions. H.V. acknowledges the Ministry of Education, Government of India, for financial support through the Prime Minister’s Research Fellowship. A.A. acknowledges funding from the Core Research Grant by ANRF (Sanction No. CRG/2023/007003), Department of Science and Technology, India.

## APPENDIX

### A1: Generalized Onsager reciprocity and dissipative nonlinear transport

Onsager reciprocity in nonmagnetic systems follows from microscopic reversibility, a consequence of time-reversal symmetry of the Hamiltonian together with equilibrium statistical mechanics. In linear response, Onsager reciprocity imposes strict constraints on transport coefficients and forbids longitudinal NCT in the absence of magnetic order or external magnetic fields.

In a nonlinear response, the second-order current generated by an electric field can be written as  $J_i(\omega_1 + \omega_2) = \sum_{jk} \sigma_{ijk}(\omega_1, \omega_2) E_j(\omega_1) E_k(\omega_2)$ . Since the charge current is odd under time reversal, microscopic reversibility implies the generalized Onsager relation in Matsubara frequency [6, 9]:  $\sigma_{ijk}(i\omega_1, i\omega_2) = -\sigma_{ikj}(-i\omega_2, -i\omega_1)$ . If the dc limit were analytic, taking  $\omega_1, \omega_2 \rightarrow 0$  would yield  $\sigma_{ijk}(0, 0) = -\sigma_{ijk}(0, 0)$ , apparently implying  $\sigma_{ijk}(0, 0) = 0$ , and forbidding any second-order dc response in a time-reversal-symmetric system.

This conclusion does not hold once momentum relaxation and dissipation are included. The dc nonlinear response corresponds to a nonequilibrium steady state that necessarily requires dissipation, which is encoded in the collision integral of the Boltzmann equation. As a result, the nonlinear conductivity develops nonanalytic structures of the form

$$\sigma_{ijk}(\omega_1, \omega_2) \sim \frac{1}{\omega_1 + i/\tau}, \quad \frac{1}{\omega_2 + i/\tau}, \quad \frac{1}{\omega_1 + \omega_2 + i/\tau}, \quad (7)$$

and their products. After analytic continuation  $i\omega \rightarrow \omega + i0^+$ , these generate relaxation poles at  $\omega_i = 0$ . The limits  $\omega_1 \rightarrow 0$  and  $\omega_2 \rightarrow 0$  therefore do not commute, and the dc response cannot be obtained by a smooth analytic continuation from Matsubara frequencies.

Physically, these poles encode the relaxation dynamics that stabilize the nonequilibrium steady state. The emergence of such nonanalytic structures is a generic feature of steady-state transport, where relaxation processes balance the external driving field. Consequently, dissipative nonlinear dc responses are not constrained by equi-

librium Onsager reciprocity relations. Longitudinal NCT proportional to  $E^2$  are therefore allowed in time-reversal-symmetric systems when inversion symmetry is broken, and the response is intrinsically dissipative.

### A2: Microscopic reversibility, detailed balance, and asymmetric scattering

Understanding longitudinal NCT in time-reversal-symmetric systems requires distinguishing between *microscopic reversibility* and *detailed balance*. These concepts are closely related but not identical. If the Hamiltonian preserves time-reversal symmetry ( $\mathcal{T}$ ), the scattering probability has to satisfy the condition of microscopic reversibility,  $w_{\mathbf{k}\rightarrow\mathbf{k}'} = w_{-\mathbf{k}'\rightarrow-\mathbf{k}}$ . This relation states that the transition probability for a  $\mathbf{k} \rightarrow \mathbf{k}'$  scattering is equal to that of the time-reversed scattering process  $-\mathbf{k}' \rightarrow -\mathbf{k}$ .

In many simplified treatments, such as the relaxation-time approximation, we further assume symmetric scattering with  $w_{\mathbf{k}\rightarrow\mathbf{k}'} = w_{\mathbf{k}'\rightarrow\mathbf{k}}$ . This enforces equality between forward and backward processes. However, this is a stronger constraint than microscopic reversibility, and it does not hold in inversion-broken systems. In such materials, the scattering probability can contain an antisymmetric component that gives rise to skew scattering. In general, the scattering rate can be decomposed into symmetric and antisymmetric parts as shown in Eq. (3). The antisymmetric part produces skew scattering and is essential for generating nonlinear nonreciprocal transport. The presence of such asymmetric scattering does not violate time-reversal symmetry because the microscopic reversibility condition remains satisfied. More importantly, we show below that such antisymmetric scattering terms also maintain detailed balance.

The principle of detailed balance follows from the requirement that the Boltzmann collision integral vanishes in equilibrium. For elastic impurity scattering, the collision integral takes the form

$$I[f(\mathbf{k})] = \sum_{\mathbf{k}'} [w_{\mathbf{k}'\rightarrow\mathbf{k}} f_{\mathbf{k}'} - w_{\mathbf{k}\rightarrow\mathbf{k}'} f_{\mathbf{k}}]. \quad (8)$$

In equilibrium, the distribution function is the Fermi-Dirac function  $f^{(0)}(\varepsilon_{\mathbf{k}})$ . For elastic scattering we have  $\varepsilon_{\mathbf{k}} = \varepsilon_{\mathbf{k}'}$ , which implies  $f_{\mathbf{k}}^{(0)} = f_{\mathbf{k}'}^{(0)}$ . Substituting this into Eq. (8) gives

$$I[f_{\mathbf{k}}^{(0)}] = f_{\mathbf{k}}^{(0)} \sum_{\mathbf{k}'} [w_{\mathbf{k}'\rightarrow\mathbf{k}} - w_{\mathbf{k}\rightarrow\mathbf{k}'}]. \quad (9)$$

For equilibrium to be maintained, the collision integral must vanish, which requires  $\sum_{\mathbf{k}'} w_{\mathbf{k}'\rightarrow\mathbf{k}} = \sum_{\mathbf{k}'} w_{\mathbf{k}\rightarrow\mathbf{k}'}$ . This is the condition of detailed balance, which states that the total probability of scattering into a state equals the total probability of scattering out of that state. The

symmetric part of the scattering rate always satisfies this detailed balance relation. Additionally, we can use the microscopic reversibility relation,  $w_{\mathbf{k}\rightarrow\mathbf{k}'} = w_{-\mathbf{k}'\rightarrow-\mathbf{k}}$ , to show that the antisymmetric scattering rate satisfies  $\sum_{\mathbf{k}'} w_{\mathbf{k}'\rightarrow\mathbf{k}}^A = \sum_{\mathbf{k}'} w_{\mathbf{k}\rightarrow\mathbf{k}'}^A = 0$ . This ensures that the total inflow and outflow scattering probabilities are equal, ensuring  $I[f^{(0)}] = 0$ .

Thus, even when the scattering probability contains an antisymmetric component responsible for skew scattering, equilibrium is preserved and no current flows. Asymmetric scattering, therefore, remains fully consistent with time-reversal symmetry and detailed balance.

### A3: Band-geometric origin of extrinsic contributions

The side-jump velocity and the antisymmetric (skew) scattering rate are the key microscopic mechanisms responsible for longitudinal NCT in time-reversal-symmetric systems. Both quantities originate from overlaps between Bloch states at different crystal momenta. In particular, the side-jump velocity explicitly depends on the intraband Berry connection through the coordinate shift of the electronic wave packet. This observation naturally suggests that even disorder-driven responses can encode geometric information of the Bloch bands. To explicitly analyze this connection, we introduce a model for the impurity potential.

#### Impurity potential modeling

To evaluate extrinsic responses associated with side-jump and skew-scattering processes, we consider randomly distributed short-range static scatterers following Refs. [34, 41, 50, 65–67]. We consider short-range impurities and model them using a Dirac-delta potential,

$$V_{\text{imp}}(\mathbf{r}) = \sum_j V_j \delta(\mathbf{r} - \mathbf{R}_j). \quad (10)$$

Here,  $V_j$  denotes the impurity strength at position  $\mathbf{R}_j$ , and the summation runs over all impurity sites. For this potential, the matrix element in the Bloch basis takes the form  $V_{ll'} \equiv V_{\mathbf{k},\mathbf{k}'}^0 \langle u_l | u_{l'} \rangle$ , where  $V_{\mathbf{k},\mathbf{k}'}^0 = \sum_j V_j e^{i(\mathbf{k}' - \mathbf{k}) \cdot \mathbf{R}_j}$  is the Fourier transform of the impurity potential. Therefore, the disorder averages of different orders of  $V_{ll'}$  required for side-jump velocity and antisymmetric scattering rate, can be written as

$$\begin{aligned} \langle V_{ll'} V_{l'l} \rangle_{\text{dis}} &= \langle V_{\mathbf{k}\mathbf{k}'}^0 V_{\mathbf{k}'\mathbf{k}}^0 \rangle_{\text{dis}} \langle u_l | u_{l'} \rangle \langle u_{l'} | u_l \rangle, \\ \langle V_{ll''} V_{l''l'} V_{l'l} \rangle_{\text{dis}} &= \langle V_{\mathbf{k}\mathbf{k}''}^0 V_{\mathbf{k}''\mathbf{k}'}^0 V_{\mathbf{k}'\mathbf{k}}^0 \rangle_{\text{dis}} \times \\ &\quad \langle u_l | u_{l''} \rangle \langle u_{l''} | u_{l'} \rangle \langle u_{l'} | u_l \rangle, \\ \langle V_{ll''} V_{l''l'} V_{l'l'''} V_{l''l} \rangle_{\text{dis}} &= \langle V_{\mathbf{k}\mathbf{k}'''}^0 V_{\mathbf{k}'''\mathbf{k}''}^0 V_{\mathbf{k}''\mathbf{k}'}^0 V_{\mathbf{k}'\mathbf{k}}^0 \rangle_{\text{dis}} \\ &\quad \times \langle u_l | u_{l'''} \rangle \langle u_{l'''} | u_{l''} \rangle \langle u_{l''} | u_{l'} \rangle \langle u_{l'} | u_l \rangle. \end{aligned}$$

For disorder averaging, we simplify

$$\begin{aligned}\langle V_{\mathbf{k}\mathbf{k}'}^0 V_{\mathbf{k}'\mathbf{k}}^0 \rangle_{\text{dis}} &= n_i V_0^2, \\ \langle V_{\mathbf{k}\mathbf{k}'}^0 V_{\mathbf{k}''\mathbf{k}'}^0 V_{\mathbf{k}'\mathbf{k}}^0 \rangle_{\text{dis}} &= n_i V_1^3, \\ \langle V_{\mathbf{k}\mathbf{k}'}^0 V_{\mathbf{k}''\mathbf{k}'}^0 V_{\mathbf{k}'\mathbf{k}'''}^0 V_{\mathbf{k}'''\mathbf{k}}^0 \rangle_{\text{dis}} &= n_i^2 V_0^4.\end{aligned}$$

Here,  $n_i$  denotes the impurity concentration, while  $V_0$  and  $V_1$  represent the zeroth and first moments of the impurity potential.

For numerical calculations, we adopt realistic disorder parameters following Ref. [41]:  $n_i \approx 10^{10} \text{ cm}^{-2}$  and  $V_0 = 6.2 \times 10^{-13} \text{ eV cm}^2$ . These values correspond to a symmetric scattering time  $\tau \approx 10^{-13} \text{ s}$  ( $\tau \approx 0.1 \text{ ps}$ ), consistent with previous studies [31, 65]. To obtain comparable magnitudes of the nonlinear skew-scattering contributions originating from third- and fourth-order processes, we set  $V_1 = 0.5V_0$ .

*Berry curvature dependence of side-jump velocity and antisymmetric scattering rate*

Following the analysis of Ref. [50], compact expressions for the side-jump velocity and skew-scattering rates can be obtained in the weak-impurity-potential limit, where both quantities acquire a direct dependence on the Berry curvature. For time-reversal-symmetric systems, the extrinsic sidejump velocity, and third and fourth order skew scattering rate are given by,

$$\begin{aligned}\mathbf{v}_{n,\mathbf{k}}^{\text{sj}} &= \frac{2\pi}{\hbar} n_i V_0^2 \mathcal{D}_n(\varepsilon_n^{\mathbf{k}}) [\mathbf{k} \times \boldsymbol{\Omega}_n], \\ w_{n,\mathbf{k}\mathbf{k}'}^{(3),A} &= \frac{2\pi^2}{\hbar} n_i V_1^3 \mathcal{D}_n(\varepsilon_n^{\mathbf{k}}) [(\mathbf{k} \times \mathbf{k}') \cdot \boldsymbol{\Omega}_n] \delta(\varepsilon_n^{\mathbf{k}} - \varepsilon_n^{\mathbf{k}'}), \\ w_{n,\mathbf{k}\mathbf{k}'}^{(4),A} &= \frac{2\pi^2}{\hbar} n_i^2 V_0^4 \mathcal{D}_n(\varepsilon_n^{\mathbf{k}}) [(\mathbf{k} \times \mathbf{k}') \cdot \tilde{\boldsymbol{\Omega}}_n] \delta(\varepsilon_n^{\mathbf{k}} - \varepsilon_n^{\mathbf{k}'}).\end{aligned}\quad (11)$$

Here  $\boldsymbol{\Omega}_n$  denotes the Berry curvature of the  $n$ th band, while  $\tilde{\boldsymbol{\Omega}}_n = \sum_{n'} \boldsymbol{\Omega}_{nn'} / (\varepsilon_n^{\mathbf{k}} - \varepsilon_{n'}^{\mathbf{k}'})$  represents the energy-normalized Berry curvature. The quantity  $\mathcal{D}_n(\varepsilon_n^{\mathbf{k}}) = \sum_{\mathbf{k}'} \delta(\varepsilon_n^{\mathbf{k}} - \varepsilon_n^{\mathbf{k}'})$  is the density of states of the  $n$ th band evaluated at energy  $\varepsilon_n^{\mathbf{k}}$ .

These gauge-invariant expressions show that both the side-jump velocity and the antisymmetric scattering rate are fundamentally controlled by the Berry curvature of the Bloch bands, which peak near the band edges. Consequently, even though these mechanisms originate from impurity scattering, their magnitude and structure are directly governed by the underlying Berry curvature of the bands.

---

\* hvarshny@iitk.ac.in

† amitag@iitk.ac.in

- [1] G. L. J. A. Rikken, J. Fölling, and P. Wyder, Electrical magnetochiral anisotropy, *Phys. Rev. Lett.* **87**, 236602 (2001).
- [2] F. Pop, P. Auban-Senzier, E. Canadell, G. L. J. A. Rikken, and N. Avarvari, Electrical magnetochiral anisotropy in a bulk chiral molecular conductor, *Nature Communications* **5**, 3757 (2014).
- [3] R. Wakatsuki, Y. Saito, S. Hoshino, Y. M. Itahashi, T. Ideue, M. Ezawa, Y. Iwasa, and N. Nagaosa, Nonreciprocal charge transport in noncentrosymmetric superconductors, *Science Advances* **3**, e1602390 (2017).
- [4] S. Hoshino, R. Wakatsuki, K. Hamamoto, and N. Nagaosa, Nonreciprocal charge transport in two-dimensional noncentrosymmetric superconductors, *Phys. Rev. B* **98**, 054510 (2018).
- [5] Y. M. Itahashi, T. Ideue, Y. Saito, S. Shimizu, T. Ouchi, T. Nojima, and Y. Iwasa, Nonreciprocal transport in gate-induced polar superconductor SrTiO<sub>3</sub>, *Science Advances* **6**, eaay9120 (2020).
- [6] N. Nagaosa and Y. Yanase, Nonreciprocal transport and optical phenomena in quantum materials, *Annual Review of Condensed Matter Physics* **15**, 63–83 (2024).
- [7] S. Dash and P. Padhan, Nonlinear hall effect and nonreciprocal charge transport in two-dimensional electron gas at the si-sio<sub>x</sub>-zno interface, *Advanced Functional Materials* **35** (2025).
- [8] S. Nagahama, Y. Sato, M. Kawamura, I. Belopolski, R. Yoshimi, A. Tsukazaki, N. Kanazawa, K. S. Takahashi, M. Kawasaki, and Y. Tokura, Control of nonreciprocal charge transport in topological insulator/superconductor heterostructures by fermi level tuning and superconducting layer thickness, *Phys. Rev. B* **112**, L121110 (2025).
- [9] T. Morimoto and N. Nagaosa, Nonreciprocal current from electron interactions in noncentrosymmetric crystals: roles of time reversal symmetry and dissipation, *Scientific Reports* **8**, 2973 (2018).
- [10] Y. Tokura and N. Nagaosa, Nonreciprocal responses from non-centrosymmetric quantum materials, *Nature Communications* **9** (2018).
- [11] T. Ideue, K. Hamamoto, S. Koshikawa, M. Ezawa, S. Shimizu, Y. Kaneko, Y. Tokura, N. Nagaosa, and Y. Iwasa, Bulk rectification effect in a polar semiconductor, *Nature Physics* **13**, 578–583 (2017).
- [12] K. Yasuda, T. Morimoto, R. Yoshimi, M. Mogi, A. Tsukazaki, M. Kawamura, K. S. Takahashi, M. Kawasaki, N. Nagaosa, and Y. Tokura, Large non-reciprocal charge transport mediated by quantum anomalous hall edge states, *Nature Nanotechnology* **15**, 831–835 (2020).
- [13] F. Ando, Y. Miyasaka, T. Li, J. Ishizuka, T. Arakawa, Y. Shiota, T. Moriyama, Y. Yanase, and T. Ono, Observation of superconducting diode effect, *Nature* **584**, 373–376 (2020).
- [14] Y. Li, Y. Li, P. Li, B. Fang, X. Yang, Y. Wen, D.-x. Zheng, C.-h. Zhang, X. He, A. Manchon, Z.-H. Cheng, and X.-x. Zhang, Nonreciprocal charge transport up to room temperature in bulk rashba semiconductor  $\alpha$ -gete, *Nature Communications* **12** (2021).
- [15] Z. Zhang, N. Wang, N. Cao, A. Wang, X. Zhou, K. Watanabe, T. Taniguchi, B. Yan, and W.-b. Gao, Controlled large non-reciprocal charge transport in an intrinsic magnetic topological insulator mnbi<sub>2</sub>te<sub>4</sub>, *Nature Communications* **13** (2022).

- [16] C. Ye, X. Xie, W. Lv, K. Huang, A. J. Yang, S. Jiang, X. Liu, D. Zhu, X. Qiu, M. Tong, T. Zhou, C.-H. Hsu, G. Chang, H. Lin, P. Li, K. Yang, Z. Wang, T. Jiang, and X. Renshaw Wang, Nonreciprocal transport in a bilayer of  $\text{mnbi}_2\text{te}_4$  and  $\text{pt}$ , *Nano Letters* **22**, 1366–1373 (2022).
- [17] N. Wang, D. Kaplan, Z. Zhang, T. Holder, N. Cao, A. Wang, X. Zhou, F. Zhou, Z. Jiang, C. Zhang, S. Ru, H. Cai, K. Watanabe, T. Taniguchi, B. Yan, and W. Gao, Quantum-metric-induced nonlinear transport in a topological antiferromagnet, *Nature* **621**, 487–492 (2023).
- [18] C. Li, R. Wang, S. Zhang, Y. Qin, Z. Ying, B. Wei, Z. Dai, F. Guo, W. Chen, R. Zhang, B. Wang, X. Wang, and F. Song, Observation of giant non-reciprocal charge transport from quantum hall states in a topological insulator, *Nature Materials* **23**, 1208–1213 (2024).
- [19] Y. Wang, Z. Zhang, Z.-G. Zhu, and G. Su, Intrinsic nonlinear ohmic current, *Phys. Rev. B* **109**, 085419 (2024).
- [20] M. Suárez-Rodríguez, F. de Juan, I. Souza, M. Gobbi, F. Casanova, and L. E. Hueso, Nonlinear transport in non-centrosymmetric systems, *Nature Materials* **24**, 1005–1018 (2025).
- [21] D. Nakamura, M.-K. Lee, K. Karube, M. Mochizuki, N. Nagaosa, Y. Tokura, and Y. Taguchi, Nonreciprocal transport in a room-temperature chiral magnet, *Science Advances* **11** (2025).
- [22] G. L. J. A. Rikken and P. Wyder, Magnetoelectric anisotropy in diffusive transport, *Phys. Rev. Lett.* **94**, 016601 (2005).
- [23] K. K. Meng, J. K. Chen, J. Miao, X. G. Xu, and Y. Jiang, Interface-driven electrical magnetochiral anisotropy in  $\text{pt}/\text{ptmng}$  bilayers, *Applied Physics Letters* **118**, 252403 (2021).
- [24] Y. Jiang, Q. Yi, and B. Yan, Electrical magnetochiral anisotropy and quantum metric in chiral conductors, *2D Materials* **12**, 015020 (2024).
- [25] H. J. Zhao, L. Tao, Y. Fu, L. Bellaiche, and Y. Ma, General theory for longitudinal nonreciprocal charge transport, *Phys. Rev. Lett.* **133**, 096802 (2024).
- [26] X. Chen, Y. Fu, X. Wang, Y. Sui, H. J. Zhao, and L. L. Tao, Magnetic control of nonreciprocal charge transport, *Phys. Rev. B* **111**, 155411 (2025).
- [27] Y. Gao, S. A. Yang, and Q. Niu, Field induced positional shift of bloch electrons and its dynamical implications, *Phys. Rev. Lett.* **112**, 166601 (2014).
- [28] K. Das and A. Agarwal, Intrinsic hall conductivities induced by the orbital magnetic moment, *Phys. Rev. B* **103**, 125432 (2021).
- [29] A. Gao, Y.-F. Liu, J.-X. Qiu, B. Ghosh, T. V. Trevisan, Y. Onishi, C. Hu, T. Qian, H.-J. Tien, S.-W. Chen, M. Huang, D. Bérubé, H. Li, C. Tzschaschel, T. Dinh, Z. Sun, S.-C. Ho, S.-W. Lien, B. Singh, K. Watanabe, T. Taniguchi, D. C. Bell, H. Lin, T.-R. Chang, C. R. Du, A. Bansil, L. Fu, N. Ni, P. P. Orth, Q. Ma, and S.-Y. Xu, Quantum metric nonlinear hall effect in a topological antiferromagnetic heterostructure, *Science* **381**, 181–186 (2023).
- [30] X. Chen, M. Dou, Q. Zhang, X. Wang, M. Y. Zhuravlev, A. V. Nikolaev, and L. L. Tao, Magnetic control of nonlinear transport induced by the quantum metric, *Phys. Rev. B* **112**, 174408 (2025).
- [31] C. Xiao, Y.-X. Huang, and S. A. Yang, Lorentz skew scattering and giant nonreciprocal magneto-transport, *Nature Communications* (2026).
- [32] X. F. Lu, X.-J. Zhang, N. Wang, J. Cao, D. Zhao, H. Wang, T. Wu, X. H. Chen, S. Lai, C. Xiao, S. A. Yang, and W. Gao, Lorentz skew scattering nonreciprocal magneto-transport, *arXiv* , 2511.03273 (2025).
- [33] K. Das, S. Lahiri, R. B. Atencia, D. Culcer, and A. Agarwal, Intrinsic nonlinear conductivities induced by the quantum metric, *Phys. Rev. B* **108**, L201405 (2023).
- [34] Z. Z. Du, C. M. Wang, S. Li, H.-Z. Lu, and X. C. Xie, Disorder-induced nonlinear hall effect with time-reversal symmetry, *Nature Communications* **10** (2019).
- [35] S. Datta, S. Bhowmik, H. Varshney, K. Watanabe, T. Taniguchi, A. Agarwal, and U. Chandni, Nonlinear electrical transport unveils fermi surface malleability in a moiré heterostructure, *Nano Letters* **24**, 9520–9527 (2024).
- [36] S. Wang, W. Niu, and Y.-W. Fang, Nonlinear hall effect in two-dimensional materials, *Microstructures* **5** (2025).
- [37] J. Smit, The spontaneous hall effect in ferromagnetics I, *Physica* **21**, 877 (1955).
- [38] J. Smit, The spontaneous hall effect in ferromagnetics II, *Physica* **24**, 39–51 (1958).
- [39] L. Berger, Side-jump mechanism for the hall effect of ferromagnets, *Phys. Rev. B* **2**, 4559 (1970).
- [40] C. Ortix, Nonlinear hall effect with time-reversal symmetry: Theory and material realizations, *Advanced Quantum Technologies* **4** (2021).
- [41] D. Ma, A. Arora, G. Vignale, and J. C. W. Song, Anomalous skew-scattering nonlinear hall effect and chiral photocurrents in  $\mathcal{PT}$ -symmetric antiferromagnets, *Phys. Rev. Lett.* **131**, 076601 (2023).
- [42] H. Isobe, S.-Y. Xu, and L. Fu, High-frequency rectification via chiral bloch electrons, *Science Advances* **6**, eaay2497 (2020).
- [43] P. He, G. K. W. Koon, H. Isobe, J. Y. Tan, J. Hu, A. H. C. Neto, L. Fu, and H. Yang, Graphene moiré superlattices with giant quantum nonlinearity of chiral bloch electrons, *Nature Nanotechnology* **17**, 378 (2022).
- [44] T. Ahmed, H. Varshney, B. Q. Tu, K. Watanabe, T. Taniguchi, M. Gobbi, F. Casanova, A. Agarwal, and L. E. Hueso, Detecting lifshitz transitions using nonlinear conductivity in bilayer graphene, *Small* **21** (2025).
- [45] M. Huang, Z. Wu, X. Zhang, X. Feng, Z. Zhou, S. Wang, Y. Chen, C. Cheng, K. Sun, Z. Y. Meng, and N. Wang, Intrinsic nonlinear hall effect and gate-switchable berry curvature sliding in twisted bilayer graphene, *Phys. Rev. Lett.* **131**, 066301 (2023).
- [46] G. Sundaram and Q. Niu, Wave-packet dynamics in slowly perturbed crystals: Gradient corrections and berry-phase effects, *Phys. Rev. B* **59**, 14915 (1999).
- [47] N. W. Ashcroft and N. D. Mermin, *Solid State Physics* (Holt-Saunders, 1976).
- [48] See Supplemental Material for a detailed discussion on (S1) Semiclassical theory of the linear and nonlinear charge transport, (S2) Tight-binding model of Bernal-stacked bilayer graphene, (S3) Low-energy analysis of bilayer graphene around the Dirac point, (S4) Relation between nonlinear conductivities and nonlinear voltages, and (S5) Disorder scaling of the nonreciprocity factor.
- [49] N. A. Sinitsyn, Q. Niu, and A. H. MacDonald, Coordinate shift in the semiclassical boltzmann equation and the anomalous hall effect, *Phys. Rev. B* **73**, 075318 (2006).
- [50] H. Varshney and A. Agarwal, Asymmetric scattering drives large nonlinear nernst and seebeck effects, *arXiv* , 2601.17775 (2026).

- [51] R. E. Newnham, *Properties of Materials: Anisotropy, Symmetry, Structure* (Oxford University Press, 2004).
- [52] S. V. Gallego, J. Etxebarria, L. Elcoro, E. S. Tasci, and J. M. Perez-Mato, Automatic calculation of symmetry-adapted tensors in magnetic and non-magnetic materials: a new tool of the Bilbao Crystallographic Server, *Acta Crystallographica Section A* **75**, 438 (2019).
- [53] Q. Ma, S.-Y. Xu, H. Shen, D. MacNeill, V. Fatemi, T.-R. Chang, A. M. Mier Valdivia, S. Wu, Z. Du, C.-H. Hsu, S. Fang, Q. D. Gibson, K. Watanabe, T. Taniguchi, R. J. Cava, E. Kaxiras, H.-Z. Lu, H. Lin, L. Fu, N. Gedik, and P. Jarillo-Herrero, Observation of the nonlinear hall effect under time-reversal-symmetric conditions, *Nature* **565**, 337–342 (2018).
- [54] D. Kumar, C.-H. Hsu, R. Sharma, T.-R. Chang, P. Yu, J. Wang, G. Eda, G. Liang, and H. Yang, Room-temperature nonlinear hall effect and wireless radiofrequency rectification in weyl semimetal tairte4, *Nature Nanotechnology* **16**, 421–425 (2021).
- [55] B. Cheng, Y. Gao, Z. Zheng, S. Chen, Z. Liu, L. Zhang, Q. Zhu, H. Li, L. Li, and C. Zeng, Giant nonlinear hall and wireless rectification effects at room temperature in the elemental semiconductor tellurium, *Nature Communications* **15**, 5513 (2024).
- [56] M. Suárez-Rodríguez, B. Martín-García, W. Skowroński, F. Calavalle, S. S. Tsirkin, I. Souza, F. De Juan, A. Chuvilin, A. Fert, M. Gobbi, F. Casanova, and L. E. Hueso, Odd nonlinear conductivity under spatial inversion in chiral tellurium, *Phys. Rev. Lett.* **132**, 046303 (2024).
- [57] M. Huang, Z. Wu, J. Hu, X. Cai, E. Li, L. An, X. Feng, Z. Ye, N. Lin, K. T. Law, and N. Wang, Giant nonlinear hall effect in twisted bilayer wse2, *National Science Review* **10**, nwac232 (2022).
- [58] J. Duan, Y. Jian, Y. Gao, H. Peng, J. Zhong, Q. Feng, J. Mao, and Y. Yao, Giant second-order nonlinear hall effect in twisted bilayer graphene, *Phys. Rev. Lett.* **129**, 186801 (2022).
- [59] S. Sinha, P. C. Adak, A. Chakraborty, K. Das, K. Debnath, L. D. V. Sangani, K. Watanabe, T. Taniguchi, U. V. Waghmare, A. Agarwal, and M. M. Deshmukh, Berry curvature dipole senses topological transition in a moiré superlattice, *Nature Physics* **18**, 765–770 (2022).
- [60] X. F. Lu, C.-P. Zhang, N. Wang, D. Zhao, X. Zhou, W. Gao, X. H. Chen, K. T. Law, and K. P. Loh, Nonlinear transport and radio frequency rectification in bitebr at room temperature, *Nature Communications* **15**, 10.1038/s41467-023-44439-w (2024).
- [61] E. McCann and M. Koshino, The electronic properties of bilayer graphene, *Reports on Progress in Physics* **76**, 056503 (2013).
- [62] A. B. Kuzmenko, I. Crassee, D. van der Marel, P. Blake, and K. S. Novoselov, Determination of the gate-tunable band gap and tight-binding parameters in bilayer graphene using infrared spectroscopy, *Phys. Rev. B* **80**, 165406 (2009).
- [63] K. Ghorai, S. Das, H. Varshney, and A. Agarwal, Planar hall effect in quasi-two-dimensional materials, *Phys. Rev. Lett.* **134**, 026301 (2025).
- [64] The displacement field is related to the onsite potential difference through  $\Delta = eDc/\epsilon_0\epsilon_r$ , where  $c = 0.335$  nm is the interlayer spacing and  $\epsilon_r \approx 2.6$  is the effective dielectric constant of BLG [? ]. The experimental range  $D/\epsilon_0 = [-0.2, -0.3, -0.5]$  V/nm therefore corresponds to  $\Delta \approx [-0.02, -0.04, -0.06]$  eV.
- [65] M. Papaž and L. Fu, Enhanced anomalous nernst effect in disordered dirac and weyl materials, *Phys. Rev. B* **103**, 075424 (2021).
- [66] R. Guo, Y.-X. Huang, X. Yang, Y. Liu, C. Xiao, and Z. Yuan, Extrinsic contribution to nonlinear current induced spin polarization, *Phys. Rev. B* **109**, 235413 (2024).
- [67] D. Ma, Z.-F. Zhang, H. Jiang, and X. C. Xie, Quantum kinetic theory of the semiclassical side jump, skew scattering, and longitudinal velocity, *Phys. Rev. B* **112**, 045136 (2025).